SINERGI Vol. 30, No. 1, February 2026: 1-10
http://publikasi.mercubuana.ac.id/index.php/sinergi
http://doi.org/10.22441/sinergi.2026.1.001

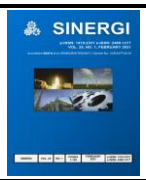

Real-time Unmanned Surface Robot (USR) for river quality monitoring system

Mohd Shahrieel Mohd Aras[1]*, Pavitrah Ponusamy[1], Mohamad Riduwan Md Nawawi[1], Fauzal Naim Zohedi[1], Mohd Bazli Bahar[1], Lokman Abdullah[2], Alias Khamis[1], Zairi Ismael Rizman[3]
[1]Faculty of Technology and Electrical Engineering, Universiti Teknikal Malaysia Melaka, Malaysia
[2]Faculty of Industrial and Manufacturing Technology and Engineering, Universiti Teknikal Malaysia Melaka, Malaysia
[3]School of Electrical Engineering, College of Engineering, Universiti Teknologi MARA, Malaysia

Abstract
A real-time Unmanned Surface Robot (USR) for river water quality monitoring system is a technology that employs a small autonomous boat outfitted with sensors and other monitoring equipment to gather and transmit data on various water quality parameters like pH, temperature and total dissolved solids sensors in rivers and other bodies of water. The USR can traverse the river, gather information or data at specific points or designated locations, as well as continuously monitor a specific stretch of river at all times. The data or information was sent in real time to a central monitoring station, where it was analyzed and used to identify potential water quality problems. Initially, the USR was designed using SolidWorks software, and its structural performance was the main focus of the investigation and examination of the design. This USR was then created and manufactured. The entire USR system could help detect and mitigate pollution and other environmental problems, as well as offer useful information for managing water resources. Next, to determine the overall performance of the USR, five experiments and autopilot accuracy tests were performed. Finally, this study also verified and validated the accuracy of water quality monitoring sensors.

Keywords:
Self-navigation;
SolidWorks design;
Unmanned surface robot;
Water quality

Article History:
Received: July 22, 2024
Revised: April 30, 2025
Accepted: July 3, 2025
Published: January 2, 2026

Corresponding Author:
Mohd Shahrieel Mohd Aras
Faculty of Technology and Electrical Engineering, Universiti Teknikal Malaysia Melaka, Malaysia
Email: shahrieel@utem.edu.my

INTRODUCTION

In Malaysia, 98% of all water consumption comes from rivers [1]. Even though Malaysia is endowed with a significant number of rivers, river pollution keeps the catchment's abundant water resources from providing a sufficient supply for all users [2, 3, 4, 5]. In general, both point and non-point sources contribute to water pollution in Malaysia. Sewage treatment facilities, manufacturing, agricultural, and livestock farms are all examples of point sources. Activities such as logging, land clearing, and earthmoving operations are responsible for non-point sources [6]. Existing River water quality monitoring systems do not get water samples from different points of the river. The major feature that a river water quality monitoring system requires is the mobility of the system to monitor water at different points of the river.

Furthermore, traditional water quality monitoring methods can be time-consuming, expensive, and limited in their ability to provide real-time data. Furthermore, manual sampling and laboratory analysis may not be feasible in some areas, such as remote or heavily polluted areas [7, 8, 9, 10]. The existing real-time river water quality systems also do not provide accurate physicochemical readings of the water. Examples of physicochemical readings are pH, total dissolved solids, dissolved oxygen, and so on. There are several problems associated with the motion control of surface robots that can affect

their ability to navigate and collect data in rivers and other bodies of water [11, 12, 13]. Maintaining a precise position in the presence of currents, waves, and wind is challenging [14]. The surface robot needs to be able to maintain a precise position to collect accurate data, and it must also be able to return to a precise position in case of an emergency. Surface robots need to be able to follow a precise trajectory to collect data on water quality parameters. This can be challenging due to the presence of currents, waves, and wind, which can cause the surface robot to deviate from its intended trajectory [15, 16, 17, 18, 19].

The purpose of this study was to design and construct an Unmanned Surface Robot (USR) for monitoring river water quality in real-time. This paper also offered a validation and verification of the water quality monitoring system's accuracy. Additionally, it examined the USR's mobility and stability characteristics.

.

Table 1. Comparison of the previous research and the research gap

Research Title	Project Description	Flight Controller Used	Type of Surface Robot	Accuracy of Sensors	Gap
Autonomous Surface Vehicle for Real-time Monitoring of Water Bodies in Bangladesh	A small autonomous hovering boat was used to monitor water bodies in Dhaka, Bangladesh.	Arduino Mega	Monohull	The accuracy of the pH sensor reading and the Turbidity sensor reading-very low	-The flight controller used is Arduino Mega, which is slower compared to pixhawk fight controller. -It also uses Monomial boat, which will be less stable compared to a catamaran. -The accuracy is low as well.
Design and Implementation of an Unmanned Surface Vehicle for Water Quality Monitoring	The unmanned surface vehicle was designed with enhanced intelligence and maneuverability to monitor river water quality.	ARM Cortex-M3 with an STM32F103ZE	Multihull Catamaran	Accuracy of water quality sensors-not mentioned	-The ARM Cortex-M3 used is which is slower compared to pixhawk fight controller. -The accuracy of the sensor is not measured in this research
A Design of Radio-controlled Submarine Modification for River Water Quality Monitoring	The flow of domestic, agricultural, and industrial water into rivers prompted the development of the radio-controlled river water quality monitoring submarine.	ARM F4 and Raspberry Pi B+	Submarine	Accuracy of water quality sensors-not mentioned	-The type of vehicle built in this research is a submarine, whereas our objective is to build a Surface Robot. -The accuracy of the sensor is not measured in this research

Table 2. Comparison between Types of Boat Propeller and Rudder Configuration

Types of Boat Propeller and Rudder Configuration	Advantages	Disadvantages
Single Propeller Single Rudder System	This configuration is simpler and less expensive than a twin rudder twin propeller system, and it can be more efficient in certain situations, such as when operating in calm waters or at a steady speed.	This configuration has limited maneuverability. With only one rudder and one propeller, the vessel is less able to make tight turns or perform evasive maneuvers.
Twin Propeller and Twin Rudder System	This configuration can provide increased maneuverability and control, as well as redundancy in case of failure. It also allows for independent control of the speed and direction of each propeller, which can be useful in certain situations such as docking or station keeping.	This configuration is more complicated than a single-rudder, single-propeller system and the twin-rudder, twin-propeller system is typically heavier.
Twin Propeller System	Twin propellers provide enhanced maneuverability, allowing the boat to make tight turns and navigate in confined spaces more easily. Each propeller can operate independently, enabling better control over the boat's movement. With two engines, twin propeller boats offer redundancy. If one engine fails or experiences a problem, the other engine can still keep the boat operational and help you reach your destination or return safely to shore.	Win propeller boats generally consume more fuel than single-engine boats due to the increased power and weight. This can result in higher operating costs, especially during long trips or when operating at higher speeds.

Table 3. Comparison between Types of Boats

Type of Boats	Operating Principle	Advantages	Disadvantages
Airboat	Uses a propeller above the boat and maneuvers around using wind force	Airboat Favored when a higher level of persistence is required and energy independence is desired	Not suitable for rough water condition. Limited range due to fuel consumption.
Catamaran	Uses rudders to change its direction of movement and an underwater thruster for propulsion.	Increased ability to maneuver and power to resist currents	Higher cost compared to other types of surface robots.
Sailboat	Utilize a sail to convert the wind's energy into a propulsion force.	Can operate with no emissions or fuel consumption. Can navigate through light wind condition	Limited speed and maneuverability compared to motorized vessels.

Mechanical Design of an Unmanned Surface Robot

Table 1 shows a comparison of the previous research and research gaps [20, 21, 22, 23] in terms of flight controller, surface robot type, and sensor used. Three previous studies were covered, along with their research gaps.

Configuration

Table 2 shows the comparison between a single propeller single rudder and twin propeller twin rudder system for the surface robot [24, 25, 26, 27]. Table 3 shows the comparison between types of boat such as airboats, catamarans, and sailboats.

RESULTS AND DISCUSSION

Results Unmanned Surface Robot Design Using Fusion 360

The catamaran-style robot's boat and structure were designed using Fusion 360. A Surface Boat's Fusion 360 design entailed building a thorough 3D model that precisely depicted the boat's components, construction, and functionality.

The initial step in the design process was shaping the hull, made up of two parallel hulls

According to Figure 1, the surface robot was shaped like a catamaran-style boat. For added buoyancy, both sides had twin hulls. Underframes connected the two hulls and offer room for sensor installation. Two thrusters were on the surface robot. The surface robot possessed the following dimensions: The boat's overall dimensions were 809mm in length, 718.24mm in width, and 223.51mm in height. The surface boat's isometric measurements are shown in Figure 2.

connected by a deck or crossbeam. Using Fusion 360's modeling capabilities, the designer may create the desired catamaran shape while keeping stability, hydrodynamics, and aesthetics in mind. The application allows for precise adjustments to dimensions, angles, and curves in order to get the required performance characteristics.

Creating comprehensive documentation and drawings for the surface robot is made simpler using Fusion 360. This entails developing assembly instructions, exploded views, and dimensions to streamline the construction and production processes. The surface robot is shown in an exploded view in Figure 1.

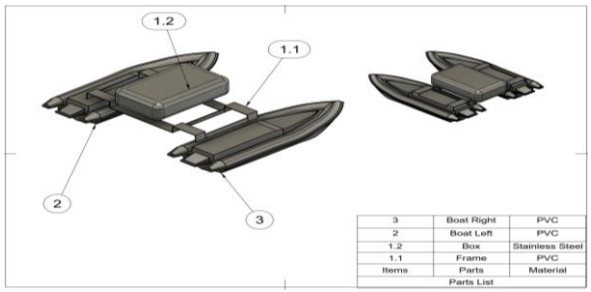

Figure 1. Exploded View of Surface Boat

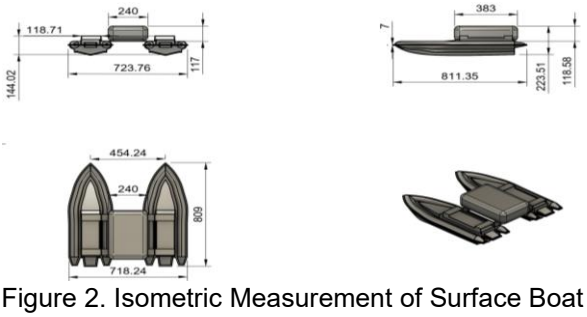

Figure 2. Isometric Measurement of Surface Boat

Circuit Design for River Monitoring System Sensor

Figure 3 shows the circuit diagram of the river water quality monitoring system. The system consisted of sensors that measured the pH level, TDS level, and temperature of the river water. These sensors were connected to a microcontroller board, such as Arduino or Raspberry Pi, which acted as the central processing unit.

To ensure a stable power supply, a step-down buck converter was used to regulate the voltage if needed. To transmit the collected data to a base station, a telemetry module was employed. This module established a communication link between the remote monitoring system and the base station. It was connected to the microcontroller board through the appropriate communication interface.

The telemetry module converted the sensor readings into digital data and formatted it according to the chosen communication protocol. The data packets containing the sensor readings were then sent via the telemetry module to the base station.

At the base station, the transmitted data was received by using a compatible telemetry module. The received data packets were processed to extract the sensor readings for further analysis.

To integrate the system with the Blynk IoT cloud, an account was created on the Blynk platform, and a new project was set up. Widgets such as gauges, graphs, and buttons were added in the Blynk app to visualize and interact with the sensor data. An authentication token was generated for the Blynk project to establish a connection with the Blynk IoT cloud. A code was implemented on the microcontroller board to read the sensor data, format it, and send it to the base station via the telemetry module. The Blynk library was used to integrate the Blynk IoT cloud into the code, enabling the transmission of sensor data.

The data was sent to the Blynk IoT cloud by using the generated authentication token. With the system set up, the Blynk app could be accessed on a mobile device to connect to the Blynk IoT cloud. The sensor data was available in the app and the added widgets allowed users to visualize and interact with the data. The pH level, TDS level and temperature of the river water could be monitored in real-time through the Blynk app.

Hardware Design of an Unmanned Surface Robot

The completed hardware design for a surface robot is displayed in Figure 4. When the surface robot was empty, its mass was 1.65 kg. PVC was selected as the boat's material, and stainless steel was selected for the structure. PVC is frequently used in the construction of boats and boxes because of its lightweight, durability, and resistance to corrosion. It maintains the vehicle's overall weight low while offering exceptional structural strength. The surface vehicle's lightweight design enhances its speed, agility, and fuel efficiency.

The boat frame was made of stainless steel because of its great strength, resistance to corrosion, and durability. It ensured the vehicle could endure a variety of operating circumstances and outside forces by providing stability and structural support to important portions of the frame. Due to its superior corrosion resistance, stainless steel is especially well-suited for applications where the frame will be exposed to seawater or harsh maritime environments.

The boat included buoyancy chambers within each hull. These chambers were sealed compartments that provided additional buoyancy to maintain the vehicle's floatability even in the event of damage or water ingress. They enhanced the overall safety and stability of the surface vehicle.

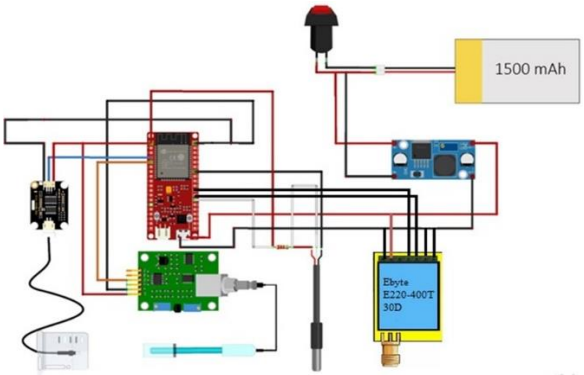

Figure 3. Circuit Diagram of River Water Quality Monitoring Sensors

Figure 4. Hardware Design of an Unmanned Surface Robot

Experiment 1: Flysky FS-IA6B Receiver Range Test

The experiment conducted was a range test for the Flysky FS-IA6B receiver, aiming to determine the maximum distance at which the receiver can successfully receive signals from the controller. The test was carried out in different scenarios involving varying distances and obstacles between the receiver and the transmitter (controller). The experiment started at a distance of 50 meters, with the receiver placed in a clear space. In this scenario, the receiver successfully connected to the transmitter, indicating that the signal was able to reach the receiver without any obstacles present. Next, the experiment introduced obstacles between the receiver and transmitter, retaining a distance of 50 meters. The receiver remained connected in this scenario as well, indicating that the signal was able to penetrate the obstacles and reached the receiver. The experiment then proceeded to test the range at a greater distance of 100 meters, while maintaining the obstacles between the receiver and transmitter. In this case, the receiver became disconnected, suggesting that the signal was no longer able to overcome the obstacles and reach the receiver at this distance.

To further investigated the range, the test was continued at a distance of 200 meters. Surprisingly, the receiver was able to connect successfully at this distance, even with the obstacles present. This suggests that the signal was able to reach the receiver despite the increased distance.

Finally, the experiment pushed the range to 224 meters (line of sight), without any obstacles between the receiver and transmitter. At this distance, the receiver became disconnected, indicating that the maximum range of the Flysky FS-IA6B receiver in clear line of sight conditions is 224 meters. Overall, the range test experiment demonstrated the maximum distance at which the receiver could receive signals from the controller. It showed that the receiver could successfully connect at distances up to 200 meters with obstacles present, but disconnected beyond that distance. However, in clear line of sight conditions, the receiver's maximum range was determined to be 224 meters. Table 4 indicates the FS-IA6B receiver range test.

Table 4. FS-IA6B Receiver Range Test Result

Distance (m)	Connectivity of Receiver on Clear Space	Connectivity of Receiver with Obstacles
50	Connected	Connected
60	Connected	Connected
70	Connected	Connected
100	Connected	Connected
200	Connected	Failsafe
224	Connected	Failsafe
226	Failsafe	Failsafe
300	Failsafe	Failsafe
400	Failsafe	Failsafe
500	Failsafe	Failsafe

Experiment 2: 433MHz Telemetry Range Test with Lora Module E220-400T30D

The experiment was to determine the maximum distance at which the Lora module E220 could send and receive data to and from a base station.

The test involved gradually increasing the distance between the transmitter and receiver while monitoring the ability to establish and maintain a connection.

The experiment began at a distance of 50 meters, where both the transmitter and receiver were able to successfully transmit and receive signals. This indicated that the communication between the two devices was functioning properly within this range. The distance was then increased, and at 272 meters, an obstacle was introduced between the receiver and transmitter. As a result, the receiver and transmitter became disconnected, indicating that the obstacle obstructed the signal and prevented a successful communication at this distance as shown in Table 5.

To further evaluated the range, the experiment continued without any obstacles between the transmitter and receiver. It was observed that the receiver remained connected even at 700 meters. This suggests that without any obstructions, the Lora module E220 could maintain a reliable connection over a considerable distance. The experiment eventually stopped at 800 meters. The decision to conclude the test at this distance was due to the availability of the testing area, specifically Ayer Keroh Lake. As the maximum distance without any obstacles that could be tested in this location was determined to be 800 meters, the experiment was concluded at that point.

In general, the experiment aimed to determine the maximum distance for data transmission via the Lora module E220. It was found that with obstacles present, the connection was lost at 272 meters. However, without any obstacles, the receiver remained connected up to a distance of 700 meters. The test was halted at 800 meters due to limitations in the available testing area.

Table 5. 433MHz Telemetry Range Test Result

Distance (m)	Connectivity of Receiver on Clear Space	Connectivity of Receiver with Obstacles
50	Connected	Connected
60	Connected	Connected
70	Connected	Connected
100	Connected	Connected
200	Connected	Connected
272	Connected	Failsafe
300	Connected	Failsafe
400	Connected	Failsafe
500	Connected	Failsafe
700	Connected	Failsafe
800	Connected	Failsafe

Experiment 3: pH Sensor and TDS Sensor Accuracy Calculation

The purpose of this experiment was to evaluate the accuracy of the pH sensor and Total Dissolved Solids (TDS) sensor. It was observed that when the TDS sensor and the pH sensor were placed together, the pH sensor readings showed significant interference. The pH sensor readings increased by more than 17 pH units, which is an incorrect value. To quantify this interference, the experiment involved placing both sensors together in buffer solutions with known fixed pH values. Three different buffer solutions were used, with pH values of 4, 6.86 and 9.18. The ADC (Analog-to-Digital Converter) readings of the pH sensor were recorded while it was positioned alongside the TDS sensor in each buffer solution. The collected data were then tabulated in Table 6, and a linear graph was plotted using the pH sensor ADC readings as the independent variable (x-axis) and the corresponding pH values as the dependent variable (y-axis). Figure 5 represents this linear graph.

By analyzing the plotted data, a linear equation was determined to represent the relationship between the pH sensor ADC readings and the accurate pH values. The obtained linear equation was y = -5.7062x + 17.505, where y represented the pH reading.

To enhance the accuracy of the pH sensor readings, this linear equation was incorporated into the ADC code of the pH sensor. By modifying the Arduino coding accordingly, the pH sensor's readings could be adjusted to compensate for the interference caused by the TDS sensor.

After editing the Arduino code, the accuracy of the pH sensor was tested once again using the buffer solutions. The aim was to verify whether the modified coding, incorporating the linear equation, improved the accuracy of the pH sensor readings. In summary, the experiment assessed the interference between the pH sensor and the TDS sensor and identified a significant increase in pH sensor readings when the two sensors were placed together. By establishing a linear equation that accounted for this interference, the accuracy of the pH sensor was enhanced. The modified Arduino code incorporating this equation enabled more accurate pH readings when tested with buffer solutions. The accuracy of pH and TDS sensors is shown in Table 7.

Experiment 4: Payload Test

A payload test for a surface robot involved assessing its capacity to carry and transport additional weight or cargo, while maintaining its stability and performance. This test helped to determine the boat's maximum payload capacity and ensure that it could handle the intended load without compromising its maneuverability or safety. To carry out the payload test, the surface robot was measured without any of its additional mass. Then, the original submerged distance of the surface robot was measured. Then, materials were added to increase the mass inside the surface boat. Then, the submerged percentage of the surface robot was measured.

Table 6. pH Sensor ADC Reading

pH Reading	Average ADC Output from pH Sensor
4	2.368
6.86	1.867
9.18	1.4596

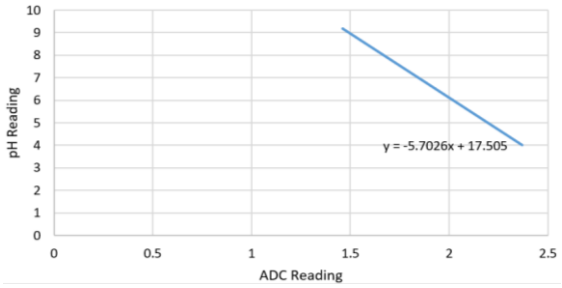

Figure 5. Linear Graph for pH Sensor ADC Reading

Table 7. pH Sensor and TDS Sensor Accuracy Table

Buffer Solution pH Value (pH)	pH Measured from the pH Sensor (pH)	pH Sensor Error	TDS Calibration Solution Value (PPT)	TDS Measure from the Sensor (PPT)	TDS Sensor Error
4.01	5.2	0.296	35	40ppt	0.1428
6.86	7.1	0.035	-	-	-
9.18	9.5	0.034	-	-	-

This process persisted until the water began to seep inside the boat. Table 8 shows the original mass of the boat was 2.5kg. The maximum weight till the water started to leak into the boat was 11.85kg where the boat was 70% submerged into the water.

Experiment 5: Turning Test

The turning test conducted on the surface robot was to measure the time taken for the robot to complete a 360-degree circle and a 180-degree circle. This test could assess the maneuverability and agility of the robot in turning movements. Table 8 presents the results of the test for a 360-degree circle. The test was conducted three times, and the time taken for each trial was recorded. To determine the average time, the three recorded times were added together, and the sum was divided by three. The average time to complete a 360-degree circle was found to be 3.25 seconds.

Similarly, Table 9 displays the results for the test conducted for a 180-degree circle. The test was also conducted three times, and the time taken for each trial was recorded. The average time was calculated by summing the three recorded times and dividing the sum by three. The average time to complete a 180-degree circle was determined to be 1.07 seconds. By conducting these turning tests and calculating the average times, the surface robot's performance in completing 360-degree and 180-degree circles can be evaluated. The shorter the average time, the quicker the robot could execute turns, indicating higher maneuverability and agility. The turning test for the surface robot involved measuring the time taken to complete a 360-degree circle and a 180-degree circle. By conducting multiple trials and calculating average times, the average time for completing each type of turn was determined. In this case, the robot took an average of 3.25 seconds to complete a 360-degree circle and 1.07 seconds to complete a 180-degree circle.

Table 8. Payload Test Result

Mass	Submerged Percentage	Water Getting in
Original mass of surface robot with frame: 2500g	10%	NO
2850	25%	NO
3850g	35%	NO
5850g	40%	NO
7850	50%	NO
9850	65%	NO
11850	70%	YES

Table 9. Time taken to complete 360 Degrees

Degree of Turning (Degrees)	Time Taken (s)
359.72	3.3
359.99	3.28
356.78	3.18
Average: 358.83	3.25

Table 10. Time taken to Complete 180 Degrees

Degree of Turning (Degrees)	Time Taken (s)
182.3	1.1
178.9	1.13
179.99	1
Average: 180.39	1.07

These times provided insights into the robot's turning capabilities and overall maneuverability. Figure 6 shows the turning test resulting from mission planner data logger which shows average of 360 degrees turn and time taken.

Sensor Reading from Ayer Keroh Lake

Figure 7 displays a graph representing the readings taken from Ayer Keroh Lake during testing. The testing was conducted from the lakebed to the middle of the lake, allowing for observations of various water parameters. At the beginning of the test, the TDS (Total Dissolved Solids) sensor reading recorded a value of 68 ppm (parts per million). This reading corresponded to an electrical conductivity (EC) of 138 µs/cm (micro-siemens per centimeter). Additionally, the pH reading was recorded at 11 units, indicating that the water was alkaline. As the surface robot reached the middle of the lake, the TDS reading increased to 130 ppm, and the EC value rose to 260 µs/cm. This suggests that the concentration of dissolved solids in the water had significantly increased in comparison to the starting point. Furthermore, the pH reading also experienced an increase, reaching a value of 12.65. This indicates a further shift towards alkalinity in the water.

Towards the end of the testing period, both the TDS and pH readings remained consistently high. This implies that the water in Ayer Keroh Lake had a substantial concentration of dissolved solids and maintained an alkaline pH level throughout the tested area. The information provided by the graph helped to assess the water quality in Ayer Keroh Lake. A higher concentration of dissolved solids, which could include different minerals, salts, or other organic and inorganic components, is suggested by the rising TDS and EC measurements. The high pH value suggests that the water is alkaline. The Blynk application's notification when the data reading beyond the predetermined limitations is displayed in Figure 8.

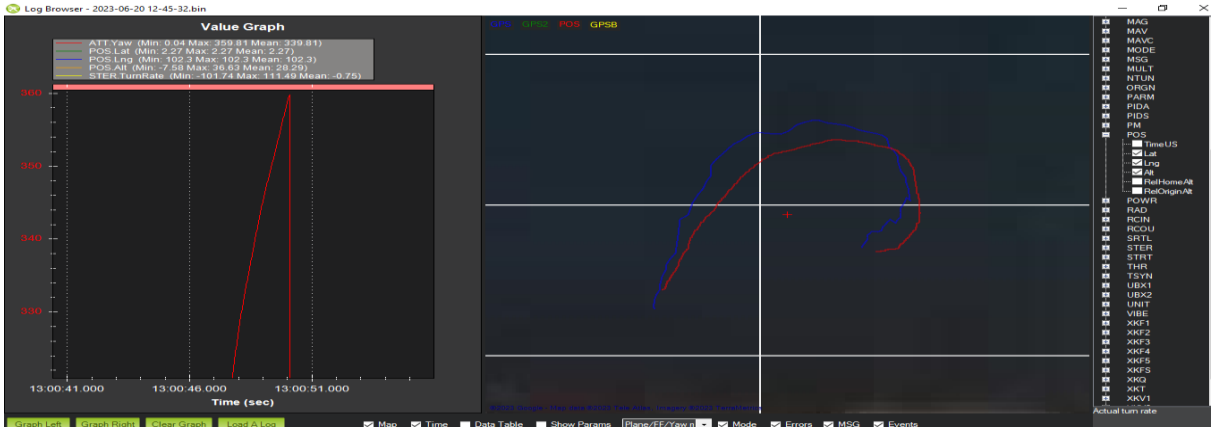

Figure 6. Turning Test Result from Pixhawk Datalogger

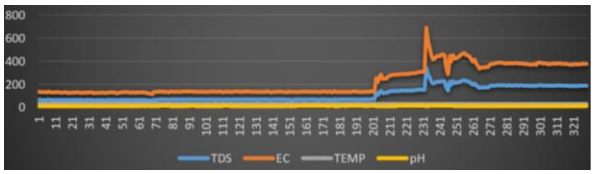

Figure 7. Reading from Lakebed to Middle of the Lake

Figure 8. Notification Received from Blynk Application When the Reading Is Abnormal

Pixhawk Autopilot Result

Figures 9 and 10 depict the results of waypoint missions carried out using a surface robot or drone. These missions involved navigating through a series of predetermined waypoints. However, the figures indicated that the waypoint missions were inaccurate, potentially deviating from the desired path.

To address this issue and improve the accuracy of the waypoint missions, the addition of a PID (Proportional-Integral-Derivative) system filter in Mission Planner was suggested. A PID system is a control loop feedback mechanism commonly used in robotics and automation to improve stability and accuracy. By implementing a PID system filter, the surface robot or drone can benefit from the improvements of proportional control. The proportional component of the PID system helps adjust the robot's navigation based on the difference between the desired waypoint location and its current position. It provides a corrective signal that is proportional to the error, helping steer the robot back on track towards the waypoints. The integral component of the PID system takes into account the accumulated error over time. It continuously adjusts the navigation by considering the historical error and applying corrective measures. This helps to address any steady-state errors or biases that may arise during the mission. The derivative component of the PID system considers the rate of change of the error. It helps provide damping and anticipates any sudden changes in the robot's position. This component aids in smoothing out the robot's movements and reducing overshoot or oscillations, resulting in more accurate navigation between waypoints.

By incorporating these PID control mechanisms into the Mission Planner software, the accuracy of the waypoint missions can be significantly enhanced. The PID system filter continuously analyzes the robot's position in relation to the desired waypoints and adjusts its navigation accordingly, ensuring precise adherence to the intended path. In summary, Figures 9 and 10 illustrate the need for increased accuracy in waypoint missions carried out by a surface robot or drone. The addition of a PID

system filter in Mission Planner is suggested to improve the robot's navigation capabilities. The PID system provides proportional, integral and derivative control mechanisms to correct errors, compensate for biases, and smooth out movements, resulting in more accurate and reliable navigation between waypoints.

Figure 9. Autopilot Test with Three Waypoints Mission

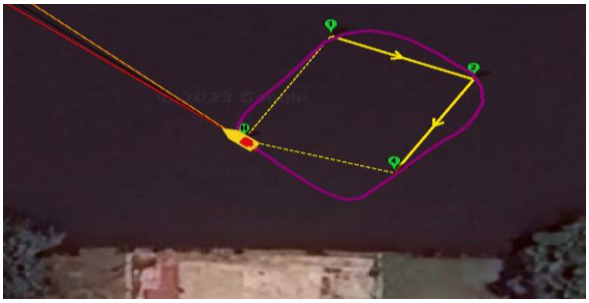

Figure 10. Autopilot Test with Four Waypoints Mission

CONCLUSION

The range tests that have been conducted in experiments one and two are crucial in establishing the operational limits of the surface robot. By progressively increasing the distance from the control station while ensuring continuous communication and control, the team successfully determines the maximum range at which the robot can effectively operates. This information provides valuable insight for planning and executing river water quality monitoring missions. Experiment three focuses on enhancing the accuracy of the water quality monitoring sensors installed on the surface robot. Through calibration and fine-tuning of sensor parameters, the team achieved higher accuracy readings by the end of the experiment. This improvement in accuracy validates the fulfillment of objective three, highlighting the successful development of a surface robot capable of providing more precise water quality data.

ACKNOWLEDGMENT

We wish to express our gratitude to the Universiti Teknikal Malaysia Melaka (UTeM) for sponsoring this work under grant: PJP/2022/FKE/S01858. Our appreciation for Faculty of Technology and Electrical Engineering (FTKE) and Underwater Technology Research Group (UTeRG) in supporting this research.

REFERENCES

[1] M. Shahbakhsh *et al.*, “Industrial revolutions and transition of the maritime industry: The case of Seafarer’s role in autonomous shipping,” *The Asian Journal of Shipping and Logistics*, vol. 38, no. 1, pp. 10-18, Mar. 2022, doi: 10.1016/j.ajsl.2021.11.004

[2] X. Wu *et al.*, “The autonomous navigation and obstacle avoidance for USVs with ANOA deep reinforcement learning method,” *Knowledge-based Systems*, vol. 196, pp. 105201, May 2020, doi: 10.1016/j.knosys.2019.105201

[3] A. Hidayat *et al.*, “Analysis of Floodwater: A Case Study of the Tukad Buluk Poh River,” *SINERGI*, vol. 28, no. 2, pp. 435-442, Jun. 2024, doi: 10.22441/sinergi.2024.2.022

[4] R. Zakariah *et al.*, “Water Pollution and Water Quality Assessment On Sungai Batang Melaka River,” *Egyptian Journal of Chemistry*, vol. 65, no. 3, pp. 245-254, Mar. 2022, doi: 10.21608/ejchem.2021.79685.3917

[5] Sarah Dickin and Sara Gabrielsson, “Inequalities in water, sanitation and hygiene: Challenges and opportunities for measurement and monitoring,” *Water Security*, Vol. 20, 2023, doi: 10.1016/j.wasec.2023.100143

[6] F. Othman *et al.*, “A Efficient river water quality index prediction considering minimal number of inputs variables,” *Engineering Applications of Computational Fluid Mechanics*, vol. 14, no. 1, pp. 751-763, Jan. 2020, doi: 10.1080/19942060.2020.1760942

[7] Ponusamy, P. et al., “Design Analysis of Unmanned Surface Robot: Preliminary Design Study,” *Lecture Notes in Electrical Engineering*, vol 1184, 2024, doi: 10.1007/978-981-97-2027-9_5

[8] Aras, M.S.M. *et al.*, ”Smart Airboat System for Water Circulation and Water Quality Monitoring,” *Lecture Notes in Electrical Engineering*, vol 1184, 2024, doi: 10.1007/978-981-97-2027-9_9

[9] F. Baharudin *et al.*, “Water Quality Index (WQI) classification of rivers in agriculture and aquaculture catchments,” *IOP Conference Series: Earth and Environmental Science, vol. 646, 3rd International Conference on Civil and Environmental Engineerin*g, Nov. 2020, pp. 012023, doi: 10.1088/1755-1315/646/1/012023

[10] G. Li *et al.*, “Fractional-Order Controller for Course-Keeping of Underactuated Surface Vessels Based on Frequency Domain Specification and Improved Particle Swarm Optimization Algorithm,” *Applied Sciences (Switzerland)*, vol. 12, no. 6, pp. 3139, Mar. 2022, doi: 10.3390/app12063139

[11] N. A. Ubina and S.-C. Cheng, “A Review of Unmanned System Technologies with Its Application to Aquaculture Farm Monitoring and Management,” *Drones*, vol. 6, no. 1, pp. 12, Jan. 2022, doi: 10.3390/drones6010012

[12] A. M. Kassim *et al.* Development of Unmanned Surface Vehicle with Real-time Water Quality Monitoring System, *2023 3rd International Conference on Computing and Information Technology (ICCIT)*, Tabuk, Saudi Arabia, 2023, pp. 567-572, doi: 10.1109/ICCIT58132.2023.10273974.

[13] I. S. M. Zawawi *et al.*, “Trend Analysis on Water Quality Index Using the Least Squares Regression Models,” *Environment and Ecology Research*, vol. 10, no. 5, pp. 561-571, 2022, doi: 10.13189/eer.2022.100504

[14] D. Efremov, “Determining the acceptable turning circle manoeuvring modes to avoid loss of efficiency of the twin propeller system,” *Maritime Technology and Research*, vol. 3, no. 2, pp. 89-101, Oct. 2020, doi: 10.33175/mtr.2021.244703

[15] N. Arish *et al.* Advancements in electrical marine propulsion technologies: A comprehensive overview," in *SAIEE Africa Research Journal*, vol. 116, no. 1, pp. 14-29, March 2025, doi: 10.23919/SAIEE.2025. 10755059.

[16] M. Terziev *et al.*, “Virtual Replica of a Towing Tank Experiment to Determine the Kelvin Half-Angle of a Ship in Restricted Water,” *Journal of Marine Science and Engineering*, vol. 8, no. 4, pp. 258, Apr. 2020, doi: 10.3390/jmse8040258

[17] R. A. Nabawi *et al.*, “Study Reduction of Resistance on The Flat Hull Ship of The Semi-Trimaran Model: Hull Vane Vs Stern Foil,” *CFD Letters*, vol. 13, no. 12, pp. 32-44, Dec. 2021, doi: 10.37934/cfdl.13.12.3244

[18] B. Piaggio *et al.*, “Twin-screw vessel manoeuvrability: The traditional twin-rudder configuration vs pod-drives,” *Ocean Engineering*, vol. 271, pp. 113725, Mar. 2023, doi: 10.1016/j.oceaneng.2023.113725

[19] R Okuda *et al.*, “Maneuvering simulations of twin-propeller and twin-rudder ship in shallow water using equivalent single rudder model.” *Journal of Marine Science and Technology*, vol. 27, no. 2, pp. 948-970, Jun. 2022, doi: 10.1007/s00773-022-00881-x

[20] J. Kustija et al., “Revitalizing IoT-based air quality monitoring system for major cities in Indonesia,” *SINERGI*, vol. 28, no. 3, p. 605-616, 2024. doi: 10.22441/sinergi.2024.3.016

[21] J. D. Setiawan *et al.*, “Development of Dynamic Model of Autonomous Sailboat for Simulation and Control,” *IEEE 7th International Conference on Information Technology, Computer, and Electrical Engineering*, Sep. 2020, pp. 52-57, doi: 10.1109/ICITACEE50144.2020.9239150

[22] M A Norazaruddin et al., ”Unmanned surface vessels in hydrographic surveying: Exploring technological progressions and development challenges,” *Indian Journal of Geo-Marine Sciences (IJMS)*, Vol. 53 No. 07, 2024. https://doi.org/10.56042/ijms.v53i07.10419

[23] D. Romahadi et al., “Intelligent System Design for Identification of Unbalance And Misalignment Using Fuzzy Logic Methods,” *SINERGI*, vol. 28, no. 2, pp. 241-250, Jun. 2024, doi: 10.22441/sinergi.2024.2.004

[24] Y. -Z. Du *et al.*, "Nonlinear Model Predictive Control for Automatic Berthing of the Underactuated Twin-propeller Twin-Rudder Ship," *IEEE Chinese Automation Congress*, Oct. 2021, pp. 3543-3548, doi: 10.1109/CAC53003.2021.9728329

[25] D. Efremov, “Determining The Asymmetric Rudder Efficiency of a Twin Rudder Patrol Ship at Manoeuvring,” *Engineering Sciences*, vol. 58, no. 2, pp. 24-43, 2021, doi: 10.7546/EngSci.LVIII.21.02.03

[26] C. Lee and J. Kim, “Trajectory Optimization for Autonomous Berthing of a Twin-Propeller Twin-Rudder Ship,” *Journal of Ocean Engineering and Technology*, vol. 37, no. 3: pp. 122-128, Jun. 2023, doi: 10.26748/KSOE.2023.013